Journal of the European Ceramic Society 23 (2003) 729–736

www.elsevier.com/locate/jeurceramsoc

Synthesis, sintering and electrical properties of $YNi_{0.33}Mn_{0.67}O_3$ perovskite prepared by a polymerized method

Carlos Moure*, Dionisio Gutierrez, Jesus Tartaj, Pedro Duran

Instituto de Cerámica y Vidrio, CSIC, Electroceramics Department, 28500 Arganda del Rey, Madrid, Spain

Received 8 February 2002; received in revised form 9 May 2002; accepted 17 May 2002

Abstract

The $YNi_{0.33}Mn_{0.67}O_3$ solid solution is a semiconducting material that shows perovskite-like structure, orthorhombic symmetry, and spatial group Pbnm. Their electrical and magnetic properties are typical of materials with potential applications in sensor systems or as cathodes in solid oxide fuel cells (SOFC's). Usually, the conventional method of mixing oxides used to obtain these materials requires high-temperature synthesis. By means of a polymerisation method (the Pechini method, slightly modified) we have obtained an amorphous, porous, and soft powder from which the $YNi_{0.33}Mn_{0.67}O_3$ solid solution can be synthesized as a single phase. The powder is characterised by a nanometric particle size and a low-temperature synthesis within the interval 750–800 °C. The formation reaction has been studied by DTA/TG analysis, X-ray diffraction (XRD) analysis and infrared absorption technique (FTIR). Also, a comparison of the sintering process and the electrical behaviour is made between the samples prepared by the chemical and the mixing oxides methods.

Keywords: Electrical properties; Perovskites; Polymerisation; Sintering; $Y(Ni,Mn)O_3$; Yttrium manganites

1. Introduction

The rare earth (RE) manganites have focused a great interest because of their electrical and magnetic properties such as semiconducting behaviour and magnetoresistive features. A lot of work has been devoted to the study of the properties of light RE manganites, which crystallises with a perovskite-type structure, particularly the $LaMnO_3$ compound modified with Ba, Sr, or Ca substituting to La cation.[1,2] The use of these solid solutions as ceramic electrodes for solid oxide fuel cells (SOFC's) has been studied for several years.[3] In the latter times, the colossal magnetoresistive effect found in both single crystals and ceramic materials based on RE manganites have been extensively treated by many authors.[4–6]

More recently, solid solutions based on the $YMnO_3$ compound, which crystallises with a different hexagonal-type structure and space group $P6_3cm$, have been studied. The incorporation of divalent small cations, such as Ni^{2+}, Co^{2+} and Cu^{2+} to the manganese sublattice induces the transition to a perovskite-type structure, like that of the light RE manganites..[7–9] The solid solutions thus obtained showed interesting electrical and magnetic features. Particularly, the $YNi_xMn_{1-x}O_3$ solid solution, $(0.20 < x < 0.50)$, with orthorhombic perovskite-type structure and space group Pbnm has a high electrical conductivity, with a maximum for $x = 0.33$.[7] The high-conductivity value and its compatibility at moderate temperatures with solid electrolytes makes it a potential material for use as ceramic electrode in Solid Oxide Fuel Cells, (SOFC's).[10] In relation to the magnetic properties, it has been observed that there is a clear shift in the effective magnetic moment for $x = x_{crit} = 0.33$, showing a constant value, independent of x, for $x < x_{crit}$ and a decreasing value against x for $x > x_{crit}$. The magnetic parameter measurements indicated that for $x < x_{crit}$ the solid solutions are antiferromagnetic and for $x > x_{crit}$ are ferromagnetic.[11]

The solid state reaction is an easy synthesis process to obtain ceramic powders of different materials. However, the homogeneity of the final synthesised powder is poor, the completion of the synthesis is only attained at very high temperatures and the particle shape and distribution

* Corresponding author. Tel.: +34-918-711800; fax: +34-918-700550.

E-mail address: cmoure@icv.csic.es (C. Moure).

0955-2219/02/$ - see front matter © 2002 Published by Elsevier Science Ltd.
PII: S0955-2219(02)00165-6

are irregular, with the presence of strong aggregates and agglomerates. The powder characteristics can be substantially improved with the use of chemical procedures for the synthesis, because of the possibility to obtain more homogeneous mixing of the reactant chemical species, lower synthesis temperature and, therefore, smaller particle sizes and a more homogeneous size distribution. These features lead to a higher reactivity and a better sinterability of powders that produces high-quality ceramic materials.

The polymerised route, based on a modification of the Pechini method,[12–14] was used to prepare $YNi_{0.33}Mn_{0.67}O_3$ solid solution powders as raw material for achieving ceramic bodies with controlled microstructure. The scope of this work is to describe the chemical process and to study the obtained powder and ceramic materials prepared by this method. The results are compared to that corresponding to a solid state reaction process.

2. Experimental procedure

$YNi_{0.33}Mn_{0.67}O_3$ powders were synthesized by the polymerised route, such as shown in Fig. 1. Individual aqueous solutions containing the required amounts of metal nitrates were prepared. Then they were mixed together to produce solutions for gel production. Separately citric acid (CA) was added to ethylene glycol (EG) in a 1/4 CA/EG molar ratio, to assure that each functional group of CA can produce the sterification process.[15] This mixture was stirred at about 40 °C to form a transparent solution. At this solution a few drops of HNO_3 were added to maintain the adequate acid degree. The aqueous solution containing the nitrates was directly mixed with the CA–EG solution. The process was carried out at 80 °C with a vigorous stirring. The transparent solution was slowly heated up to 130 °C to favour the sterification reaction, forming a dark viscous gel. The temperature was then raised up to 180 °C, maintaining the stirring. The polymeric gel thus formed is a soft resin with pores and bubbles, which are the result of the expulsion of gases derived of the solvents. The resin is easily powdered in an agate mortar. The resultant concentrated product was calcined at 270 °C for 10 h to eliminate the carbonous gases. Elimination of the other organic compound is carried out at 600 °C. Final synthesis was carried out at 800 °C for 1 h. After calcining the powder was attrition milled for 4 h in methanol, dried, granulated and then isopressed at 200 MPa. The green compacts were sintered at a constant rate heating (CRH) and cooling (2 °C/min) in a dilatometer (Netzsch 402 E/7 of Geratebau, Bayern, Germany) in the temperature range of 25–1500 °C. Only the 850–1500 °C range has been represented for a higher clearness of graphics. The oxide synthesis was performed by mixing the corresponding oxides, with a submicronic size, in an attrition mill, with isopropanol. The synthesis was carried out at 1100 °C, for 2 h. Several treatments at intermediate temperatures were also performed.

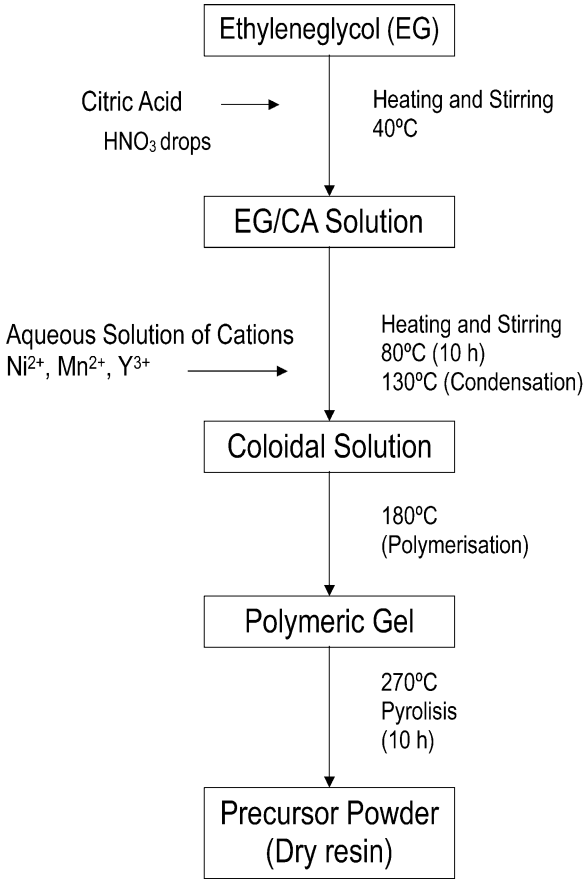

Fig. 1. Flow-chart for preparing $YNi_{0.33}Mn_{0.67}O_3$ ceramic powders.

The crystallisation process of the polymeric precursors was studied in air by thermogravimetric and differential thermal analysis, (TASC 414/2, Netzsch Geratebau, Selb. Bayern, Germany) using a heating rate of 5 °C/min. The existing phases in the sample after calcining were studied by X-ray diffraction (XRD) CuK_α, 50 kV–30 mA, (Siemens D-5000, Erlangen, Germany). Crystallite size of the calcined powder was determined by X-ray line broadening using the Scherrer equation.[16] The scan rate was 2° 2θ/min for both, phase identification and crystallite measure. A scan rate of 1/4° 2θ/min was used for determining the lattice parameters. Powder of Si was employed as internal standard. The morphology of the resin and the calcined powder was observed using a Scaning Electron Microscopy, SEM (Zeiss DSM950, Oberkochem, Germany). Specific surface area of the calcined powders was measured by the single-point BET method (Quantachrome MS-16 model, Suoset, NY). Pore size distribution in the green compacts was studied by mercury porosimetry (Micromeritics, Autopore II, 9215, Norgross, USA).

FTIR Infrared analysis spectra were obtained in a Perkin-Elmer equipment, model 1720X, using KBr as diluent of powder. Density of the sintered samples was measured by the water immersion method. The microstructure and grain size of the ceramics were observed on polished and chemically etched surfaces of sintered samples by using SEM. Four-point DC conductivity measurements were carried out for both samples between 25 and 700 °C. Bar-shaped pellets were painted with silver paste and fired at 800 °C for 1 h. For the electrical measurements, a Constant Current DC power supply (Tektronix, model PS280) and a HP Multimeter (model 44201A), with 1 μA DC current resolution was used. Activation energies were calculated from the corresponding Arrhenius plots.

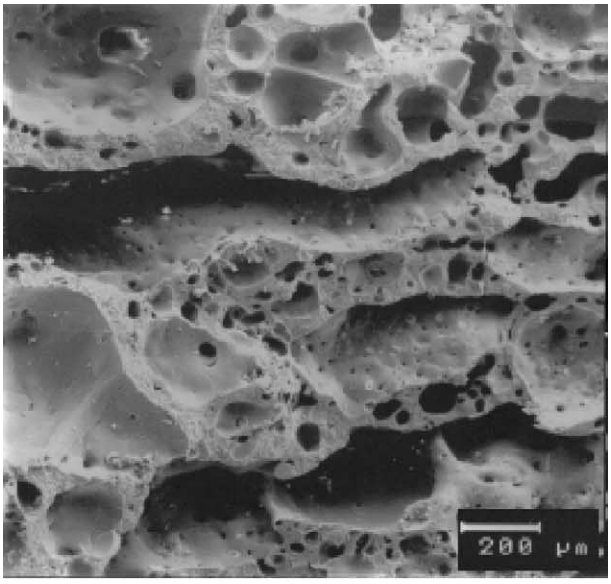

Fig. 2. SEM micrographs showing the morphology of $YNi_{0.33}Mn_{0.67}O_3$ polymeric resin precursor (a), general field and (b) detailed image, after calcining at 270 °C.

3. Results and discussion

Fig. 2 shows a SEM micrograph corresponding to the precursor resin, treated at 270 °C. It can be seen the very high porosity due to the rapid emission of gases, "puffing". Fig. 3 depicts the DTA and TG curves of the resin. At temperatures lower than 600 °C there is a wide, strong exothermal effect, which is extended from 300 to 500 °C, without continuity break. This effect is accompanied by a weight loss higher than 70%. It can be attributed to the dehidratation and evaporation process, combustion of organic compounds, cationic oxidation, possible carbonate decomposition and perhaps the beginning of perovskite crystallisation. Some of these reactions are endothermic and others are exothermic. Such as the curve is, it seems difficult to establish separately each of these different reactions. It seems that the exothermic reaction: combustion, oxidation and crystallisation are predominating on the another. Above 500 °C, the weight keeps almost constant, and no new effects are appreciate in the DTA curve up to the final temperature, 800 °C.

Taking into account those results, powdered samples were heat-treated from 600 to 800 °C, at different times in an electrical furnace, and air atmosphere. The powder samples were directly extracted from the furnace at the corresponding treatment temperatures. Fig. 4a shows the X-Ray diffraction patterns of samples subjected at different heating cycles. In each pattern, thermal conditions are indicated. The dried precursor remained amorphous up to 600 °C. It is possible to see that the perovskite phase begings to appear from the amorphous state without

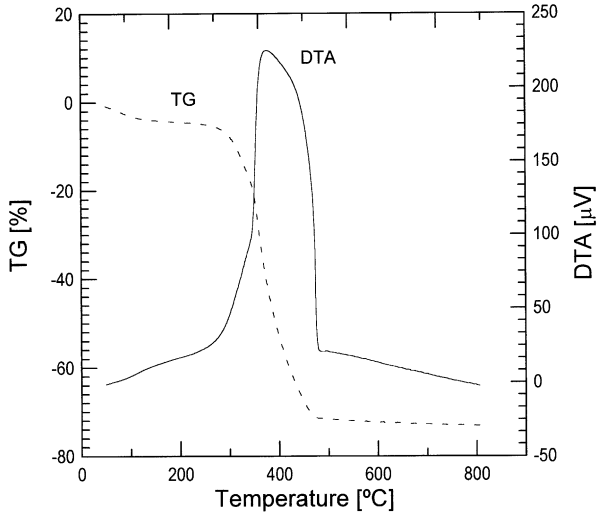

Fig. 3. TG and DTA curves $YNi_{0.33}Mn_{0.67}O_3$-citrate polymeric precursor.

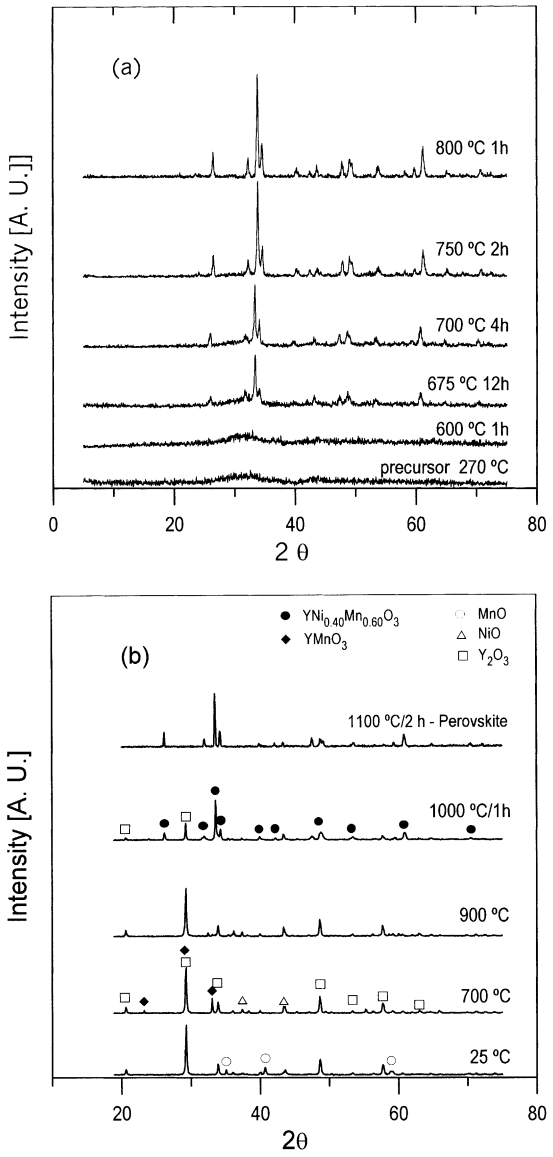

Fig. 4. XRD patterns of the $YNi_{0.33}Mn_{0.67}O_3$ powders taken at the indicated temperatures; (a) $YNi_{0.33}Mn_{0.67}O_3$ from polymeric precursor; (b) $YNi_{0.33}Mn_{0.67}O_3$ from solid state reaction.

formation of secondary phases or by-products, at 600 °C for 1 h. The perovskite is almost fully formed at 800 °C for 1h, (93% of total amount). The synthesis reaction progresses more slowly for increasing times, (see Fig. 5). Fig. 4b depicts the different steps of the reaction between the oxides. It can be seen that at 1000 °C, perovskite phase is still accompanied by other phases, such as unreacted Y_2O_3. It is necessary to attain 1100 °C, for 2 h to accomplish the almost full reaction. Table 1 shows the lattice parameter values of both sample types. The solid solution is ful accomplished and there are not differences between the two powders, i.e. the powder preparation process do not affect the crystalline structure.

Fig. 6 shows the evolution of the different steps of the perovskite formation by means of FTIR IR analysis. In

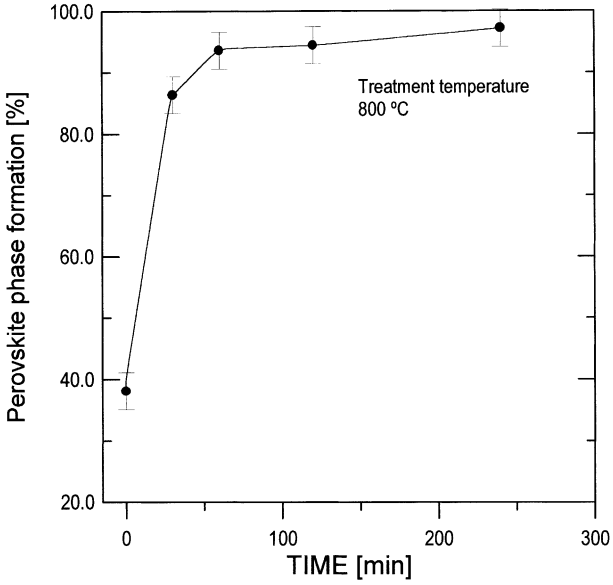

Fig. 5. Perovskite phase formation (%) as a function of time taken at 800 °C.

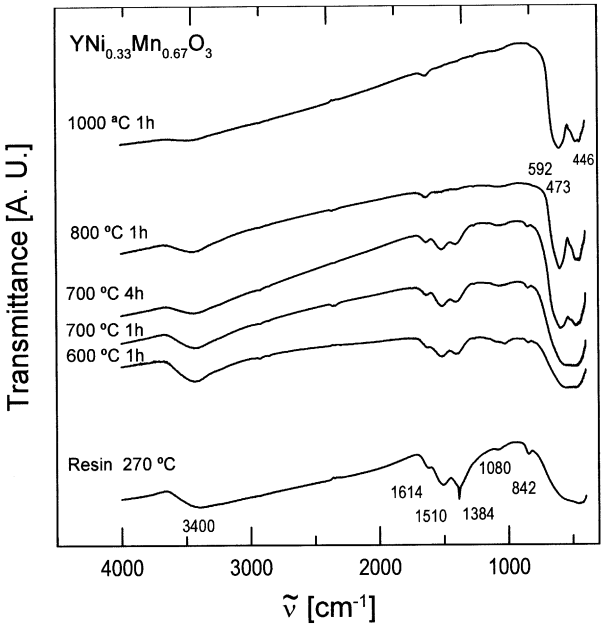

Fig. 6. Infrared spectra showing the evolution against temperature of the different chemical species from resin to fully reacting $YNi_{0.33}Mn_{0.67}O_3$.

Table 1
Lattice parameters of $YNi_{0.33}Mn_{0.67}O_3$, prepared by the chemical way and solid state reaction

Lattice parameters	Chemical way	Solid state reaction	% Difference
a (±0.0001 nm)	0,5239	0,5239	<0.01
b (±0.0001 nm)	0,5619	0,5641	<0.05
c (±0.0001 nm)	0,7459	0,7452	<0.01

the range of 3250–3750 cm^{-1} a band corresponding to O–H bonds is visible up to high temperatures. On the other hand, bands corresponding to carbon bonds, particularly carboxyl groups are visible in the 1000–3000 cm^{-1} interval. From 600 °C to above, a broad band, which is splitting in two narrower bands is appreciated at 400–600 cm^{-1} range. These bands correspond to the M–O, (M=Ni, Mn) bonds, characteristic of the perovskite structure.[17,18] These results agrees well with the obtained by DTA and X-Ray diffraction analysis.

According to these results, the precursor resin was calcined at 800 °C for 1 h. The ceramic powder thus obtained was attrition milled for 2 h, with isopropanol as the liquid medium. Fig. 7a shows a SEM micrograph taken on the as-calcined resin. It is possible to see the formation of some agglomerates. Fig. 7b corresponds to a SEM micrograph of the milled powders. The agglomerates have been broken. The apparent particle size is nanometric. BET specific surface areas measure gave a value of ~60 m^2/g, which is much higher than that measured on the oxide-way powder (~5 m^2/g) and the calculated equivalent particle size from the expression $D=6/\rho S$ (where D is the average diameter of spherical particles, S the surface area of the calcined powder and ρ the theoretical density of $YNi_{0.33}Mn_{0.67}O_3$) is 17 nm. The particle size, determined by X-Ray diffraction peak broadening was ~20 nm, which agrees well with the specific surface areas, and with the observed by SEM.

Compacted samples of both oxide (OM) and chemical prepared (CM) powders were isopressed at 200 MPa. Fig. 8 shows the pore size distribution curves, obtained by Hg porosimetry. Whereas the CM compact has a quite narrow size distribution with an average pore diameter of 45 nm, a bimodal pore size distribution curve with an average pore diameter of 210 nm for the majority mode of the OM powder compacts, was found. The smaller pores can be attributed to the intraagglomerate porosity. It is evident from the above results that the CM calcined powders consisted of soft agglomerates, which are quite easily broken down during compaction leading to uniformly packed green compacts. From the almost unimodal pore size distribution curve in these compacts, it is suggested that the step was very effective in destroying, if any, the strong agglomerates.

Fig. 9 displays the linear shrinkage and lineal shrinkage rate curves of the two kinds of powder compacts during the firing process as studied by CRH dilatometric

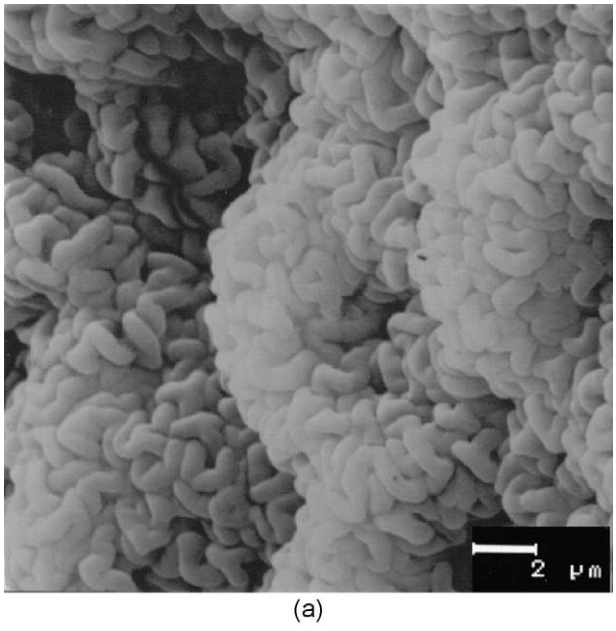

Fig. 7. SEM micrographs showing the morphology of $YNi_{0.33}Mn_{0.67}O_3$ calcined at 800 °C for 1 h; (a) as calcined; (b) after attrition milling.

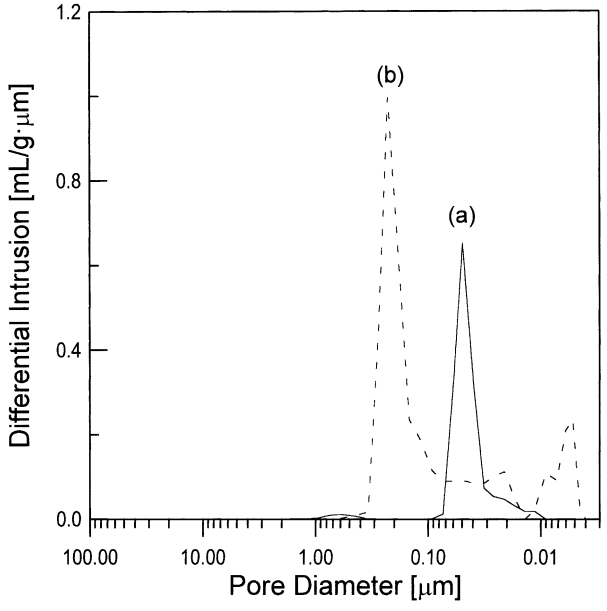

Fig. 8. Pore sizes distribution in green compacts of (a) chemically prepared (CM) and (b) oxide prepared (OM) powders.

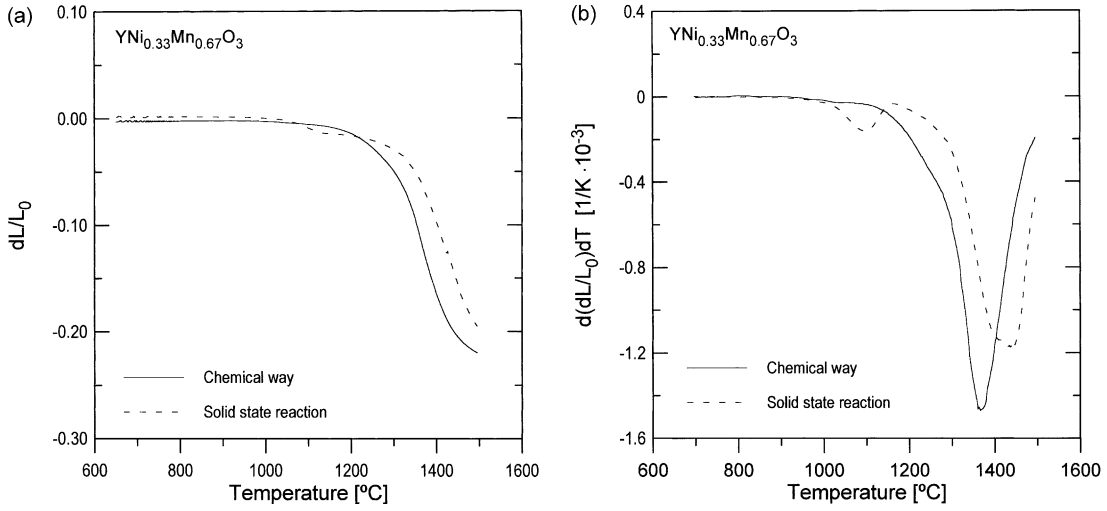

Fig. 9. (a) Shrinkage and (b) shrinkage rate behaviour of green CM and OM compacts during sintering.

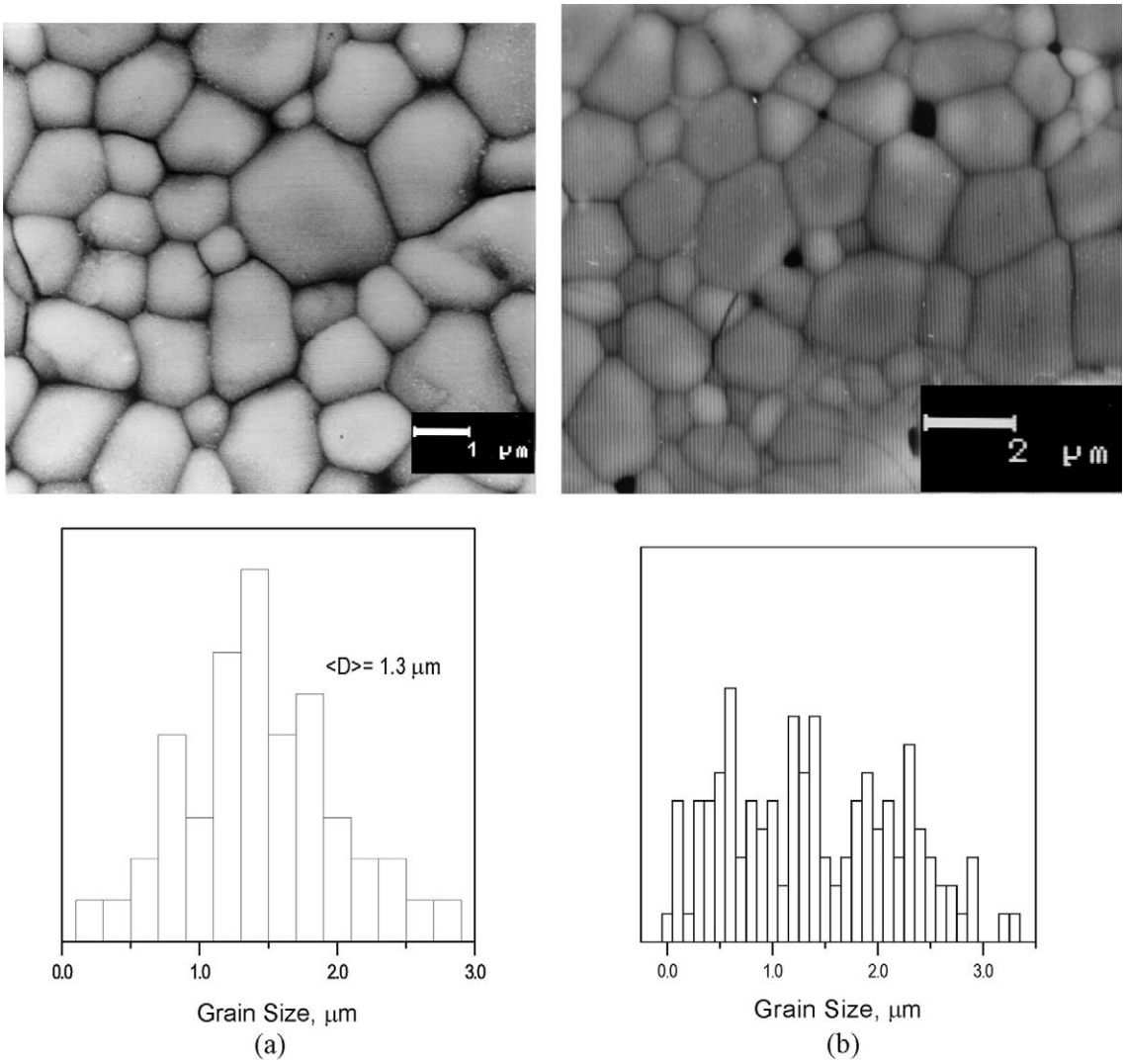

Fig. 10. Developed microstructure on sintering and grain size distribution of the CM compact, sintered at 1300 °C for 2 h (a), and the OM compact sintered at 1380 °C for 2 h (b).

measurements. Fig. 9a shows the shrinkage curve. The CM sample has the onset of shrinkage at ~1200 °C and at 1500 °C the shrinkage process is very near of its end, with a total shrinkage of 22%. The OM sample has the onset of shrinkage at a higher temperature, ~1270 °C and at 1500 °C the shrinkage end is still not attained. Fig. 9b shows the shrinkage rate curves for both samples. The CM sample presents a single maximum at the rate curve, in a strong agree with the pore size distribution and the higher uniformity of the powders. This maximum corresponds to the peak in the pore size distribution, and assuming a solid state densification mechanism at this temperature interval, the shrinkage corresponds to the elimination of that porosity. The relatively high value of the mean pore size, 46 nm, makes the temperature of the maximum shrinkage appear also at relatively high temperatures. The temperature for which the shrinkage rate is maximum is 1366 °C, with a value of -1.46×10^{-3} K^{-1}, whereas the corresponding values measured on the OM sample are 1443 and -1.18×10^{-3} K^{-1} respectively. Besides that, the OM sample shows a less homogeneous shrinkage process, with a second maximum at lower temperatures, (1100 °C), which can be attributed to the elimination of the smaller pores, which are present in the pore size distribution curve at 6 nm.

Isopressed compacts were isothermally sintered, with a heating rate of 1.5 °C and a cooling rate of 1 °C. Fig. 10a displays the SEM micrograph of the microstructure corresponding to a CM sample sintered at 1300 °C for 2 h. The apparent density was 98% D_{th}, which is higher than that measured on samples OM, with a maximum value of 94.5% D_{th} (7). The microstructure is rather homogeneous, such as can be seen in the grain size distribution graphic that is annexed. Fig. 10b shows the SEM micrograph of the microstructure corresponding to an OM sample sintered at 1380 °C for 2 h. The microstructure is more heterogeneous, with several families of grain size, such as is visible in the grain size distribution graphic. It can be seen grains with a size > 2 μm, along with grains with size < 1 μm. In average, both samples have similar grain sizes, being the CM sample more homogeneous that the OM one. Microstructural development for both CM and OM compacts seem to indicate that the liquid phase has not formed at these sintering temperatures, and solid state densification mechanism is predominant.

Fig. 11 depicts the Arrhenius plots of the conductivity vs temperature measurements. Two samples of each processing method, OM and CM have been essayed, and the curves are depicted from the average values. Log σT against $1/T$ has been represented. According to these results, the ceramic materials are semiconducting, with a thermally activated small polaron hopping as the conduction mechanism, such as was referred to in a previous work, see Ref. 7. The electrical conductivity

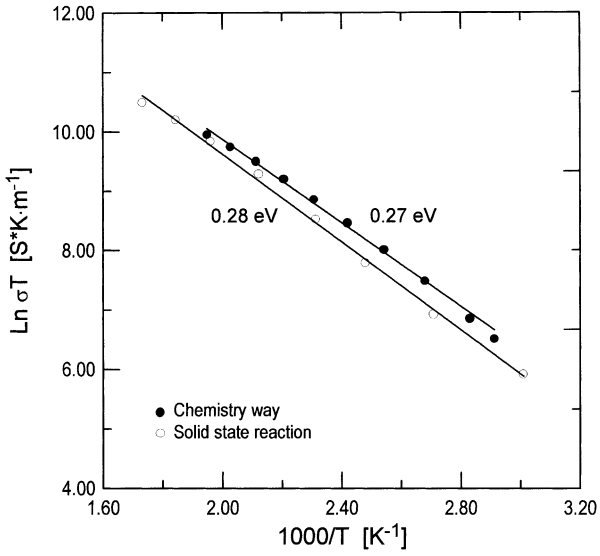

Fig. 11. LnσT against $1/T$ for both CM and OM ceramic samples.

and the activation energy are quite similar in the two samples. The conductivity is somewhat higher and the activation energy is lower for the CM ceramic samples, with regard to the OM ceramic ones. These small differences can be attributed to the higher density, homogeneity and lower sintering temperature, which probably lead to better performances.

4. Conclusions

Solid solution $YNi_{0.33}Mn_{0.67}O_3$, with a perovskite structure, has been synthesised by a polymeric precursor route. The synthesis can be performed at 800 °C, 300 °C below the temperature needed for the complete synthesis carried out by solid state reaction between the corresponding submicronic-sized oxides. The powder shows nanometric-scale size and soft agglomerates, which can be broken for attrition milling and pressing. The powder has better sinterability characteristics, and allows us to obtain dense, homogeneous grain-sized, ceramic bodies at temperatures lower than that of the solid state reaction powders. The different processes of synthesis do not affect electrical properties.

Acknowledgements

The CICYT MAT 2000–0815 programs supported this work.

References

1. Tanaka, J., Takahashi, K., Yukino, K. and Horiuchi, S., Electrical conduction of $(La_{0.80}Ca_{0.20})MnO_3$ with homogeneous ionic distribution. *Phys. Status Solidi*, 1983, **80**, 621–630.

2. Hammouche, A., Siebert, E. and Hammou, A., Crystallographic, thermal and electrochemical properties of the system $La_{1-x}Sr_xMnO_3$ for high temperature solid oxide fuel cell. *Mater. Res. Bull.*, 1989, **24**, 367–380.
3. Ostergard, M. J. L. and Mogensen, M., AC impedance study of the oxygen reduction mechanism on $La_xSr_{1-x}MnO_3$ in SOFC. *Electrochimica Acta*, 1993, **38**, 2015–2020.
4. Urishabara, A., Moritomo, Y., Arima, T., Asatmisu, A., Kido, G. and Yokura, Y., Insulator-metal transition and giant magnetoresistance in $La_{1-x}Sr_xMnO_3$. *Phys. Res.*, 1995, **B14**, 103–114.
5. Tokura, Y. and Tomioka, Y., Colossal magnetoresistive manganites. *J. Magn. Magn. Materials*, 1999, **200**, 1–23.
6. Dagotto, E., Hotta, T. A. and Moreo, A., Colossal magnetoresistant materials: the key role of phase separation. *Physics Reports*, 2001, **344**, 1–153.
7. Gutierrez, D., Peña, O., Duran, P. and Moure, C., Crystalline structure and electrical properties of solid solutions $YNi_xMn_{1-x}O_3$. *J. Eur. Ceram. Soc.*, 2002, **22**, 567–572.
8. Gutierrez, D., Peña, O., Duran, P. and Moure, C., Crystalline structure and electrical properties of solid solution $Y(Co,Mn)O_3$. *J. Eur. Ceram. Soc.*, 2002, **22**, 1257–1262.
9. Gutierrez, D., Fernandez, J. F., Peña, O. and Moure, C., Estructura cristalina y propiedades eléctricas de soluciones sólidas $YCu_xMn_{1-x}O_3$. *Bol. Soc. Esp. Ceram. Vidr.*, 2001, **40**, 211–214.
10. Moure, C., Gutiérrez, D., Tartaj, J., Capel, F. and Duran, P., Solid state compatibility between yttrium nickel manganite electrode and yttria-doped ceria and yttria-doped zirconia electrolytes. *Solid State Ionics*, 2001, **144**, 257–262.
11. Peña, O., Gutiérrez, D., Fernández, J. F., Duran, P. and Moure, C., Critical behavior in the perovskite-like system $Y(Ni,Mn)O_3$. *Journal of Physics and Chemistry of Solids*, 2000, **61**, 2019–2024.
12. Pechini, M., *Method of Preparing Lead and Coating Method Using The Same to Form a Capacitor*. US Patent No. 3 330 697, 11 July, 1967.
13. Gülgün, M. *et al.*, Polymerized organic-inorganic synthesis of mixed oxides. *J. Am. Ceram. Soc.*, 1999, **82**, 556–560.
14. Duran, P., Capel, F., Gutierrez, D., Tartaj, J., Bañares, M. A. and Moure, C., Metal citrate polymerized complex thermal decomposition leading to the synthesis of $BaTiO_3$: effectes of the precursor structure on the $BaTiO_3$ formation mechanism. *J. Mater. Chem.*, 2001, **11**, 1828–1836.
15. Lessign, A., Mixed-cation oxide powders via polymeric precursors. *Ceramic Bulletin.*, 1989, **68**(5).
16. Cullity, B. D., *Elements of X-ray Diffraction,* 2nd edn. Addison-Wesley, Reading, MA, 1978.
17. Subbarao, G. V. and Ferraro, J. R., Infrared and electronic spectra of rare earth perovskites: ortho-chromites, -manganites and ferrites. *Applied Spectroscopy.*, 1970, **24**, 436–445.
18. Couzi, M. and Huong, P. V., Spectres infrarouge et Raman des pérovskites. *Ann. Chim.*, 1974, **9**, 19–29.